Spherical Indentation of Elastic-Plastic Solids
Author(s): Sinisa Dj. Mesarovic and Norman A. Fleck
Source: *Proceedings: Mathematical, Physical and Engineering Sciences*, Vol. 455, No. 1987 (Jul. 8, 1999), pp. 2707-2728
Published by: Royal Society
Stable URL: https://www.jstor.org/stable/53493
Accessed: 31-10-2019 00:35 UTC

THE ROYAL SOCIETY

Spherical indentation of elastic-plastic solids

BY SINISA DJ. MESAROVIC† AND NORMAN A. FLECK

Department of Engineering, University of Cambridge, Trumpington Street, Cambridge CB2 1PZ, UK

Received 20 January 1998; accepted 19 October 1998

The finite-element method is used to perform an accurate numerical study of the normal indentation of an elastic-plastic half-space by a rigid sphere. The effects of elasticity and strain-hardening rate of the half-space are explored, and the role of friction is assessed by analysing the limiting cases of frictionless contact and sticking friction. Indentation maps are constructed with axes of contact radius a (normalized by the indenter radius R) and the yield strain of the half-space. Competing regimes of deformation mode are determined and are plotted on the indentation map: (i) elastic Hertzian contact; (ii) elastic-plastic deformation; (iii) plastic similarity regime; (iv) finite-deformation elastic contact; and (v) finite-deformation plastic contact. The locations of the boundaries between deformation regimes change only slightly with the degree of strain-hardening rate and of interfacial friction. It is found that the domain of validity of the rigid–strain-hardening similarity solution is rather restricted: it is relevant only for solids with a yield strain of less than 2×10^{-4} and $a/R < 0.16$. Friction between the indenter and the substrate strongly affects the strain field beneath the indenter, and has a significant effect on the contact size as a function of indent depth. The effect of pre-stress within the half-space is also explored; it is found that the indentation response is hardly affected, except for the case of the elastic-plastic indentation regime.

Keywords: indentation; finite-element method; plasticity; residual stress

1. Introduction

The contact of two non-conforming bodies is a fundamental problem in the mechanics of materials, which has a wide range of applications. For example, the friction and wear of engineering solids depend critically on the details of the contacts at asperity level. Powder compaction processes rely upon the plastic indentation of deformable particles for their success, and predictions of the multi-axial stress versus strain compaction behaviour are based on a knowledge of the local indentation response between particles. Indentation tests have been used from the beginning of this century to measure routinely the plastic properties of metals. Yet current international standards on indentation tests are based on empirical correlations, with little input from analytical and numerical solutions.

In this paper, a finite-element study of spherical indentation is reported. Only recently has contact modelling by the finite-element method advanced sufficiently,

† Present address: Department of Materials Science and Engineering, University of Charlottesville, VA 22903, USA (sm9vw@virginia.edu).

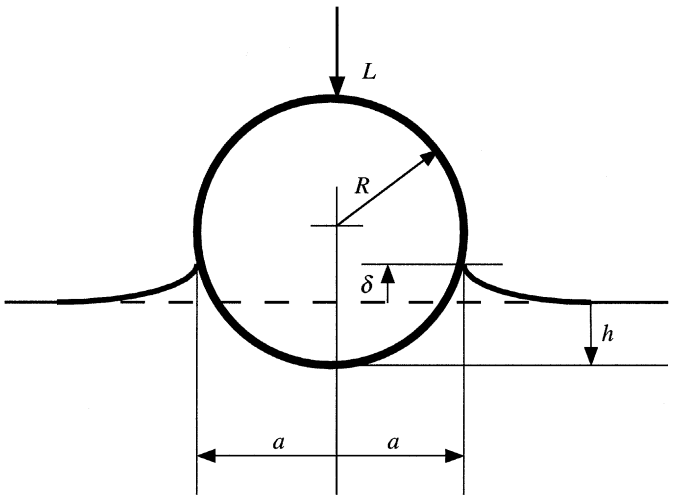

Figure 1. Geometry of spherical indentation. A normal load L is applied to the sphere of radius R, resulting in a contact radius a and indent depth h. The pile-up δ is positive if the material piles up above the initial surface of the half-space.

and the computational power become readily available, for such a study to be conducted within a practical time-scale. Previous indentation calculations were based on restrictive assumptions introduced to minimize the computational effort (see, for example, Hill *et al.* 1989; Biwa & Storåkers 1995; Bower *et al.* 1993), were limited in scope or accuracy due to the limited computational power available (Hardy *et al.* 1971; Follansbee & Sinclair 1984), or were focused on specific aspects of indentation (Fleck *et al.* 1992; Kral *et al.* 1993, 1995*a*, *b*; Ogbonna *et al.* 1995). The present study of Brinell indentation is part of a larger computational study of the contact of dissimilar spherical particles, and additional results are reported in the companion paper (Mesarovic & Fleck 1999).

We shall consider normal indentation of an elastic-plastic half-space by a rigid sphere of radius R. It is assumed that the half-space is sufficiently tough for indentation to proceed without crack formation (Sharp *et al.* 1993), and that the yield strain is sufficiently small (less than 10%) for yielding to occur before finite-deformation effects intervene. Initially, elastic indentation occurs and the classical solution of Hertz is reproduced for the frictionless indenter. Initial yield occurs when the average contact pressure (over the projected contact area) is *ca.* 10% above the yield stress of the material. Continuing indentation is characterized as elastic-plastic since both elastic and plastic deformation contribute to the overall response. Johnson (1970) has shown that the elastic-plastic mode is akin to the steady-state expansion of a spherical cavity, with a small plastic zone contained within an outer elastic field. Further indentation leads to the fully plastic regime. We show that the fully plastic regime can be subdivided into two regimes: for relatively small contact sizes, a similarity solution applies, as discussed below, while for large contact sizes, a finite-deformation mode dominates. It is the purpose of the present paper to explore in detail the regimes of dominance of the competing modes of indentation.

The geometric parameters associated with spherical (Brinell) indentation are defined in figure 1. A rigid sphere of radius R, loaded by a normal force L, indents a

semi-infinite medium to a depth h and to a contact radius a; the pile-up/sink-in at the edge of the contact with respect to the original level δ is taken to be positive for pile-up, and negative for sink-in. It is further assumed that the half-space comprises a homogeneous isotropic elastic-plastic solid, with the usual elastic parameters of Young's modulus, E, and Poisson's ratio, ν. Precise details of the plastic behaviour are given below, but, for the moment, we assume that the plastic response is characterized by two parameters: a strength σ_0 and a non-dimensional strain-hardening exponent m. Dimensional analysis reveals that the normalized contact size, a/R, and the normalized average contact pressure, $L/(\pi a^2 \sigma_0)$, depend upon the four independent non-dimensional groups of indent depth h/R, yield strain σ_0/E, and the material parameters m and ν. For small indent depths, the response is elastic and is given by the Hertz elastic solution for frictionless indentation, and by Mossakovski (1963) and Spence (1968) for a sticking indenter (for a review of these solutions see Hills *et al.* 1993). Note that in the Hertz solution, Poisson's ratio ν appears combined with the Young's modulus E in the form of a single elastic constant

$$E^* \equiv E/(1-\nu^2). \tag{1.1}$$

Experiments (Johnson 1970) and early numerical results summarized by Johnson (1985, p. 176) suggest that the elastic constant (1.1) adequately describes the elastic contribution to deformation in the elastic-plastic indentation regime.

(*a*) *The similarity solution*

With increasing indent depth, the indentation response becomes dominated by plastic flow, and it is to be expected that the elastic parameters become irrelevant; then, the non-dimensional contact size a/R and contact pressure $L/(\pi a^2 \sigma_0)$ will depend only upon non-dimensional indent depth h/R and the strain-hardening exponent m. For this regime of behaviour, a similarity solution for rigid-plastic indentation has been found by Hill *et al.* (1989). Motivated by Tabor's (1951) analysis and by a number of early experimental investigations (Meyer 1908; O'Neill 1944; Norbury & Samuel 1928), Hill *et al.* (1989) determined the similarity solution upon making the following simplifying assumptions.

(i) The constitutive law of the indented half-space is power law in nature and satisfies J_2 deformation theory. In the uniaxial case, the strain ε is a power-law function of stress σ, $\varepsilon = \varepsilon_0(\sigma/\sigma_0)^m$, where m is a strain-hardening exponent, ε_0 is a representative strain, and σ_0 is a representative strength of the solid. Note that a linear elastic contribution to deformation is neglected for the general case $m \neq 1$.

(ii) The geometric profile of the indenter can be represented by a power-law relation, for both plane strain and axisymmetric problems. This assumption includes indentation by a rigid sphere, since, for small contact sizes, the profile of a sphere can be approximated by a paraboloid of revolution.

(iii) Infinitesimal straining occurs, and, at any stage of indentation, the indenter imposes a uniform normal velocity on the current contact patch of the half-space.

Hill *et al.* (1989) showed that the overall solution has the property of self-similarity, i.e. that the geometry, stress and strain fields throughout the indentation process are derivable from a single solution by appropriate scaling. For indentation by a sphere, the appropriate scaling laws are

$$\frac{L}{\pi a^2 \sigma_0} = \alpha \left(\frac{a}{\varepsilon_0 R} \right)^{1/m} \tag{1.2a}$$

and

$$a^2 = c^2 2hR, \tag{1.2b}$$

where the functions α and c^2 depend only upon the value of m and the friction assumption, and must be determined numerically for the nonlinear solid. Suitable rearrangement of (1.2 *a*), (1.2 *b*), reveals that the load versus contact depth relation takes the power-law form

$$\frac{L\varepsilon_0^{1/m}}{\pi R^2 \sigma_0} = K(m) \left(\frac{h}{R} \right)^{[(2m+1)/2m]}, \tag{1.3a}$$

where

$$K \equiv \alpha (2c^2)^{[(2m+1)/2m]}. \tag{1.3b}$$

Hill (1992) and Bower *et al.* (1993) extended the similarity solution to the case of a power-law creeping solid, and Biwa & Storåkers (1995) extended it to the case of a J_2 flow theory solid. Bower *et al.* (1993) also considered the effects of friction between the indenter and the substrate. The above authors tabulated the values of α and c^2 for a range of hardening exponents and creep indices. Their finite-element formulations are based on the assumption of self-similarity and are, essentially, single-step solutions, where the history dependence is replaced by a spatial (radial) dependence in a modified boundary-value problem.

In the current paper, the limits of validity of the similarity solution are investigated. Specifically, the effects of elasticity and finite deformation are determined. For that purpose, selected values of the elastic and plastic constitutive parameters are assumed and different ways of coupling elastic and plastic deformation are explored. It is found that the regime of validity of the similarity solution is restricted by both elasticity and by finite-deformation effects. Indentation maps are constructed to display the competing regimes of deformation mode: elastic, elastic-plastic, plastic similarity solution, elastic-finite deformation, and plastic-finite deformation. Next, the effects of friction are examined for the limiting cases of a frictionless and a sticking indenter. Finally, the indentation response is explored for a half-space containing a pre-existing uniform stress field.

2. Constitutive description and finite-element implementation

Two hardening versions of isotropic J_2 flow theory are considered: a piecewise-linear/power-law version and a Ramberg–Osgood strain-hardening law. For both descriptions, the yield strength is defined by σ_0, the yield strain by ε_0, and the initial slope of the uniaxial stress versus strain curve defines the Young's modulus $E \equiv \sigma_0/\varepsilon_0$.

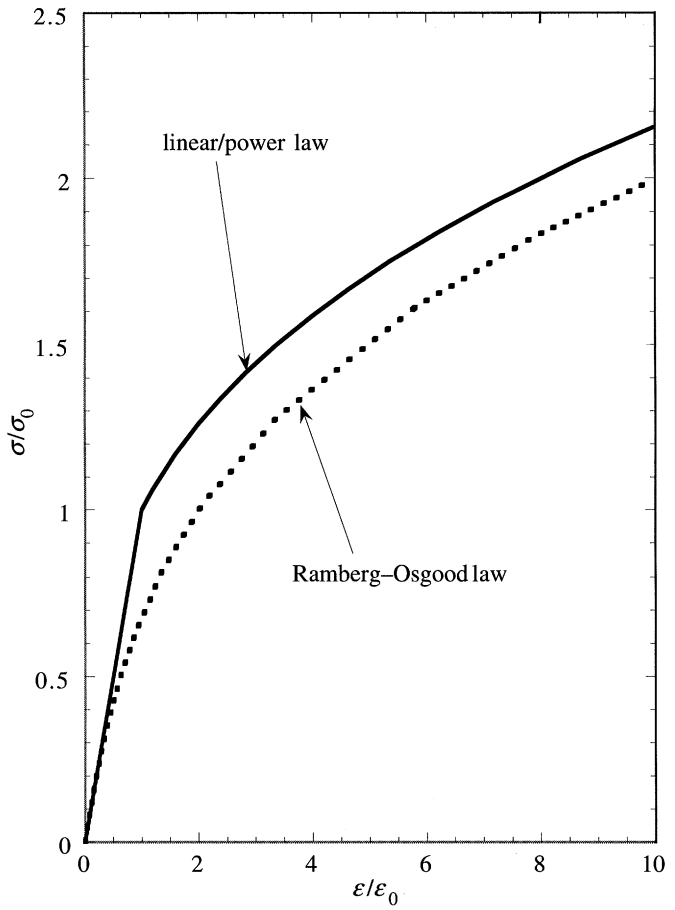

Figure 2. A choice of strain-hardening law: linear/power law described by (2.1), and Ramberg–Osgood law, described by (2.2). In both cases, curves are shown for a strain-hardening exponent $m = 3$.

(i) Piecewise-linear/power-law version. We assume that under uniaxial tension the total strain is linear in strain for $\sigma < \sigma_0$, and is power law in strain beyond the yield strength, $\sigma > \sigma_0$,

$$\frac{\varepsilon}{\varepsilon_0} = \begin{cases} \sigma/\sigma_0, & \text{for } \sigma \leqslant \sigma_0, \\ (\sigma/\sigma_0)^m, & \text{for } \sigma > \sigma_0, \end{cases} \tag{2.1}$$

where m is a strain-hardening exponent. Note that (2.1) dictates that the plastic strain vanishes below yield, and is given by $\varepsilon^{\mathrm{pl}} = \varepsilon_0[(\sigma/\sigma_0)^m - \sigma/\sigma_0]$ for $\sigma > \sigma_0$.

(ii) Ramberg–Osgood hardening law. Under uniaxial tension the total strain is given by

$$\varepsilon/\varepsilon_0 = \sigma/\sigma_0 + (\sigma/\sigma_0)^m, \tag{2.2}$$

where m is again the strain-hardening exponent. The strain-hardening laws (2.1) and (2.2) differ for small strains but converge at $\varepsilon/\varepsilon_0 \gg 1$, as sketched in figure 2.

In the elastic-ideally plastic limit, $m \to \infty$, the constitutive laws (2.1) and (2.2) coincide.

The uniaxial constitutive relations (2.1) and (2.2) are readily generalized to arbitrary stress–strain states within the framework of the J_2 flow theory by defining the effective (Mises) stress, σ, the effective strain rate $\dot{\varepsilon}$, and the effective strain, ε, according to

$$\sigma = \sqrt{\tfrac{3}{2} s_{ij} s_{ij}}, \tag{2.3a}$$

$$\dot{\varepsilon} = \sqrt{\tfrac{2}{3} D_{ij} D_{ij}}, \tag{2.3b}$$

and

$$\varepsilon(t) = \int_0^t \dot{\varepsilon}(\tau)\, \mathrm{d}\tau, \tag{2.3c}$$

where s_{ij} are the deviatoric components of the Cauchy stress, D_{ij} are the symmetric components of the velocity gradient (with respect to the current configuration), and the usual indicial notation is used.

In the current study, we concentrate on frictionless indentation of (i) an elastic-ideally plastic solid ($m \to \infty$), and (ii) the power-law hardening solids (2.1) and (2.2) with $m = 3$. Some additional runs were done for $m = 2$ and $m = 7$ in order to confirm general trends. Indentation depths of up to $h = 0.2R$ were investigated, which corresponds to $a/R = 0.7$ for an elastic-ideally plastic solid, and to $a/R = 0.5$ for the hardening solid (2.2) with $m = 3$; thus, the recommended indentation regime was covered for both the Brinell and Rockwell B tests (ASTM 1993). The effects of friction and pre-existing stress were investigated for the elastic-ideally plastic solid.

(*a*) *Finite-element implementation*

The finite-element calculations were performed using the commercial finite-element code ABAQUS (ABAQUS 1995). The rigid contact surface option was employed to mimic the rigid indenter, and finite-deformation effects were included in the formulation. A typical mesh, comprising eight-noded isoparametric rectangles and six-noded isoparametric triangles, is displayed in figure 3. Despite the differences in contact behaviour of mid-side and corner nodes, the second-order elements showed better convergence and accuracy than linear elements used in preliminary runs. The hybrid element formulation was used to facilitate convergence at large strains, where incompressible plastic deformation dominates. The mesh has over 3000 elements and about 27 000 degrees of freedom. The shortest distance between nodes along the contact is about $0.0005R$. Automatic stepping of displacement was used for most calculations except for a few special cases when the maximum increment was set manually to check the accuracy of the solution. The automatic stepping routine required between 100 and 1000 increments. (The former value was required for rapid strain hardening and a high yield strain (10^{-2}), while the latter value was required for the elastic-ideally plastic case with a low value of yield strain (10^{-5}).) Other meshes were used occasionally for specially difficult cases and to check some salient points of the solution. For example, a refined mesh was used to obtain better resolution in the elastic regime; the mesh spacing was one-third of that of the standard mesh. A mesh that

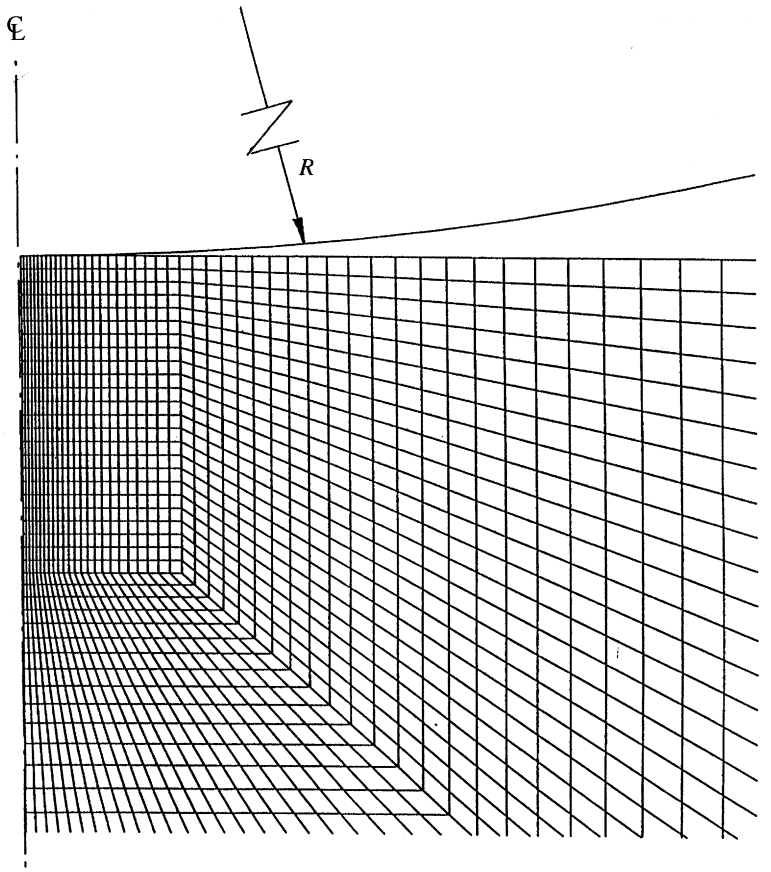

Figure 3. Typical finite-element mesh, composed of second-order isoparametric axisymmetric elements. The distance between nodes at first contact is $0.0005R$.

is refined at large contact size was used to check the accuracy of solution at large contacts.

Preliminary studies showed that the precise outer boundary conditions are unimportant for meshes with an outer boundary further than $10R$. In general, vanishing displacements were applied on the quarter-circular outer boundary at a radius of $20R$. However, for the case of a pre-stressed half-space, a square outer boundary, $20R \times 20R$, was used for the sake of simplicity; prescribed radial displacements were imposed prior to indentation along the outer edge of the square boundary, the bottom being free to move horizontally.

In addition to the usual errors associated with the numerical procedure, such as the element interpolation functions, an error specific to finite-element contact problems is due to the discrete increments in contact size (as observed by, for example, Laursen & Simo (1992) and Fleck *et al.* (1992)). To gain insight into the nature of this error, an infinitesimal strain elastic analysis was performed of frictionless indentation by a sphere, and compared with the Hertz solution. The results are shown in figure 4. Each vertical column of circular data points gives the contact size at a constant number of contact nodes. The top point of each column represents the instant when a new node makes first contact with the indenter. As indentation proceeds, the indentation depth

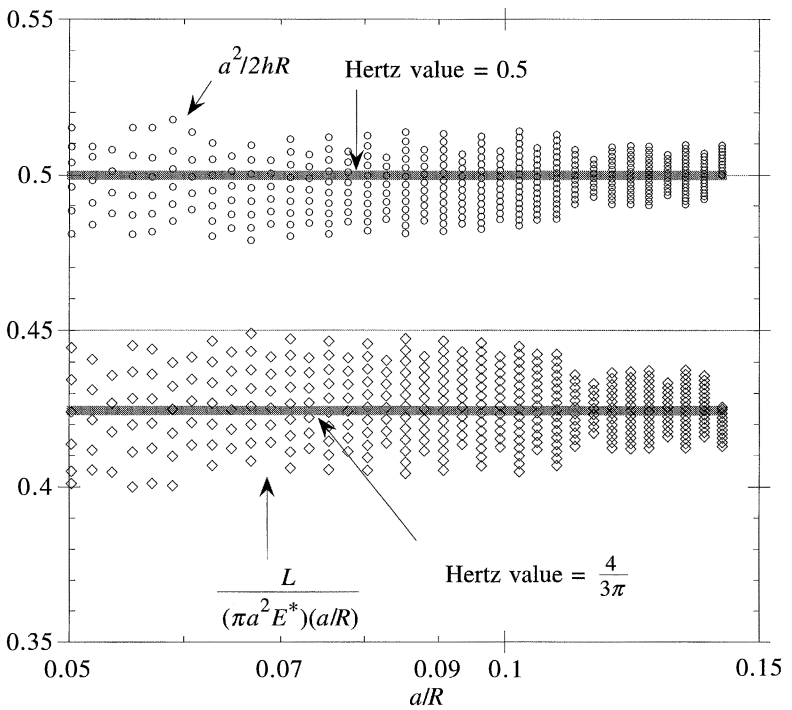

Figure 4. Comparison of finite-element results for frictionless elastic indentation and the Hertz solution. In the finite-element calculations, a value for Poisson's ratio of $\nu = 0.3$ was chosen.

h increases, but, until the next node makes contact, the contact size a remains the same in the infinitesimal strain formulation; when the finite-deformation formulation is used and sliding is allowed, the contact size increases slightly. Thus, data points appear as vertical columns. The interpretation for $L/[(\pi a^2 E^*)(a/R)]$ (diamonds) is similar: the lowermost data correspond to first contact of successive nodes. A comparison of the numerical solution with the exact Hertz solution in figure 4 shows that the midpoint of each column is close to the Hertz solution. The error in $a^2/2hR$ is less then $\pm 6\%$ for $a/R = 0.05$, and decreases to *ca.* $\pm 3\%$ for $a/R > 0.1$. Generally, one can express the relative error as one-half of the ratio of the distance between nodes and the current contact size, so that the 'worst' data reported here (for a contact size $a/R = 0.001$, with initial contact nodes spaced at $0.00017R$) have an error of $\pm 8.5\%$. The actual scatter (as in figure 4) is usually somewhat larger than the error predicted in this way, probably due to the additional errors inherent in the finite-element procedure. For clarity, only the selected midpoints are reported for the elastic-plastic cases.

3. Frictionless indentation of an elastic-ideally plastic solid

(*a*) *Average indentation pressure as a function of contact size*

The finite-element procedure was used to calculate the indentation response for normal indentation of an elastic-ideally plastic half-space by a frictionless sphere. In elastic Hertzian contact, the indentation solution depends only on the plane-strain

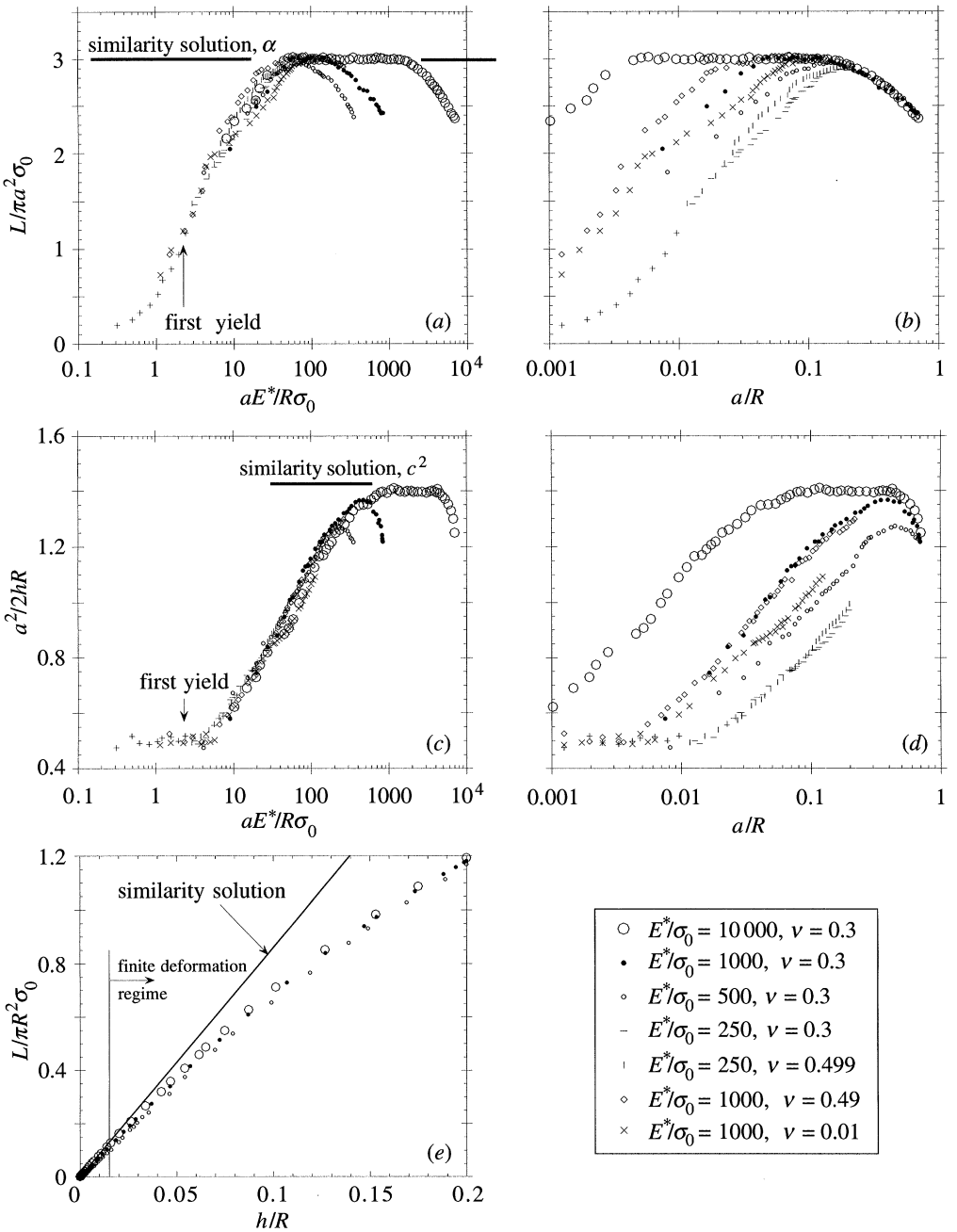

Figure 5. Frictionless indentation of an elastic-ideally plastic solid. Finite-element results and similarity solution. (*a*) Average pressure as a function of $aE^*/(R\sigma_0)$; (*b*) average pressure as a function of a/R; (*c*) $a^2/(2hR)$ as a function of $aE^*/(R\sigma_0)$; (*d*) $a^2/(2hR)$ as a function of a/R; (*e*) load versus indent depth response.

elastic modulus E^* as given by (1.1), and not on E and ν independently. Consequently, Johnson (1970) argued that in the early stages of elastic-plastic indentation, the effects of elasticity depend primarily upon the magnitude of E^*. We also make this choice, and report results in terms of E^*. Most of the runs were done with $\nu = 0.3$, except for a few cases where extreme values of Poisson's ratio were used in order to check the validity of using the single elastic constant E^*. Johnson (1970) further argued that the degree of deformation in elastic-plastic indentation depends upon the ratio of the representative strain a/R beneath the indenter to the yield strain σ_0/E^* of the half-space. Thus, the degree of indentation is defined by the single non-dimensional group $aE^*/R\sigma_0$. With this rationale in mind, finite-element predictions of the average indentation pressure are plotted against $aE^*/R\sigma_0$ in figure 5*a*, for a wide range in value of σ_0/E^* and Poisson ratio ν. The results for $aE^*/R\sigma_0 < 100$ agree with both experimental values and early numerical results given by Johnson (1970, 1985). After an initial regime of elastic Hertzian contact, the material yields at $L/\pi a^2\sigma_0 \approx 1.1$ and $aE^*/R\sigma_0 \approx 2.5$. The plot of mean pressure versus $aE^*/R\sigma_0$ shows no obvious departure from linearity at the onset of yield, and remains linear until $L/\pi a^2\sigma_0 \approx 1.6$. Thus, the parameter E^* accurately accounts for effects of elasticity beyond first yield. This is hardly surprising, since plastic flow is initially confined to a small volume of material centred at a depth of about $0.5a$. As the plastic zone spreads, the normalization by the elastic constant E^* becomes less accurate and the individual curves begin to diverge. The deviation in the responses at larger contact pressures ($L/\pi a^2\sigma_0 > 1.6$) in figure 5*a* is due to more than numerical scatter, and a dependence can be observed of the average pressure upon the Poisson ratio (and, hence, upon the elastic compressibility): the lower the elastic compressibility of the material, the higher is the average pressure.

As the contact size is increased further, the average indentation pressure increases until a regime of constant average pressure is reached at $(aE^*/R\sigma_0) = 40$–50; the plateau value of pressure is in agreement with the value predicted by the rigid-ideally plastic similarity solution (1.2 *a*). At somewhat larger values of $(aE^*/R\sigma_0)$, the average pressure falls with increasing contact size and the curves markedly separate. At these large values of contact size, the elastic contribution to the strain field beneath the indenter is negligible, and the parameter $(aE^*/R\sigma_0)$ ceases to uniquely define the degree of indentation. Instead, the normalized contact size a/R is the controlling non-dimensional parameter. This is clearly demonstrated by a plot of normalized contact pressure, $L/\pi a^2\sigma_0$ versus a/R, as shown in figure 5*b*. Therein, the curves of average pressure versus a/R coalesce to a single master curve for $a/R > 0.16$, independent of the magnitude of σ_0/E^* and of ν. For smaller values of contact size, the relative locations of the responses depend strongly upon the values of σ_0/E^* in addition to a/R, as already discussed. It is further noted from figure 5*a*, *b* that the maximum value of the average pressure associated with the similarity solution is never attained for a solid with a sufficiently high yield strain.

The drop in average pressure with increasing contact size for $a/R > 0.16$ represents the failure of the assumptions involved in the similarity solution, specifically the assumption of infinitesimal strain kinematics and the boundary condition of uniform normal velocity. As the contact size increases, the tangential velocity of points in contact with the indenter deviates from the horizontal, so that the uniform vertical velocity boundary condition ceases to be appropriate.

Most hardness measurements in metals are actually done in the finite-deformation regime (ASTM 1993). The present results are in broad agreement with Tabor's (1951, p. 51) summary of hardness measurements for work-hardened metals with a high yield strain. He found that the ratio of average contact pressure to yield strength is between 2.8 and 2.9, rather then 3, which is predicted by the similarity solution. A similar drop in the average pressure for large contacts has been observed for the compression of elastic-plastic spheres between flat elastic platens (Chaudhri *et al.* 1984; Timothy *et al.* 1987; Chaudhri 1987).

(*b*) *Contact area as a function of indent depth*

The normalized contact area $a^2/2hR$ is plotted against $(aE^*/R\sigma_0)$ in figure 5*c* and against a/R in figure 5*d*. First yield is again not detectable: $a^2/2hR$ remains constant at the value 0.5 beyond first yield until the plastic zone has spread somewhat. The elastic constant E^* appears to be the appropriate combination of elastic parameters in the elastic-plastic regime. With a further increase in contact size, the rigid-plastic similarity regime of constant $a^2/2hR$ is attained only for very low values of the yield strain (less than about 2×10^{-4}). Again, the value of a/R that marks the beginning of the finite-deformation regime is independent of the value of the elastic parameters (figure 5*d*).

The onset of the finite-deformation regime predicted here ($a/R = 0.16$) differs from the finite-element predictions of Bower *et al.* (1993), who predict that the finite-deformation effects become relevant at $a/R = 0.4$. We attribute this difference to the coarse mesh used by Bower *et al.* (1993).

(*c*) *Contact stiffness*

The relationship between indent depth and contact force is of fundamental importance in applications of indentation theory to the contact stiffness of rough surfaces and to the macroscopic compaction response of an assemblage of particles. In addition, the load–displacement relation is relevant to some types of indentation test, such as the Rockwell B test. Plots of contact load versus indent depth are given in figure 5*e*, for the same range in value of yield strain and Poisson's ratio as reported in figure 5*a–d*. The secant contact stiffness L/h is constant in the similarity regime, but decreases with increasing contact size in the finite-deformation regime, as illustrated in figure 5*e*. The drop in contact stiffness compared with the similarity solution is due to the multiplicative effect of the drop in average contact pressure, see figure 5*b*, and the drop in contact area, see figure 5*d*. Elastic deformation has a negligible effect on the load–displacement curve in the finite-deformation regime: the response is insensitive to the value of the elastic parameters within this regime.

(*d*) *Indentation map*

A map showing the various regimes of deformation for normal indentation of an elastic-ideally plastic solid by a frictionless sphere is shown in figure 6. The axes are the contact size a/R and the yield strain σ_0/E^* as independent non-dimensional variables. The contours of average pressure and the normalized contact area $a^2/2hR$ are shown.

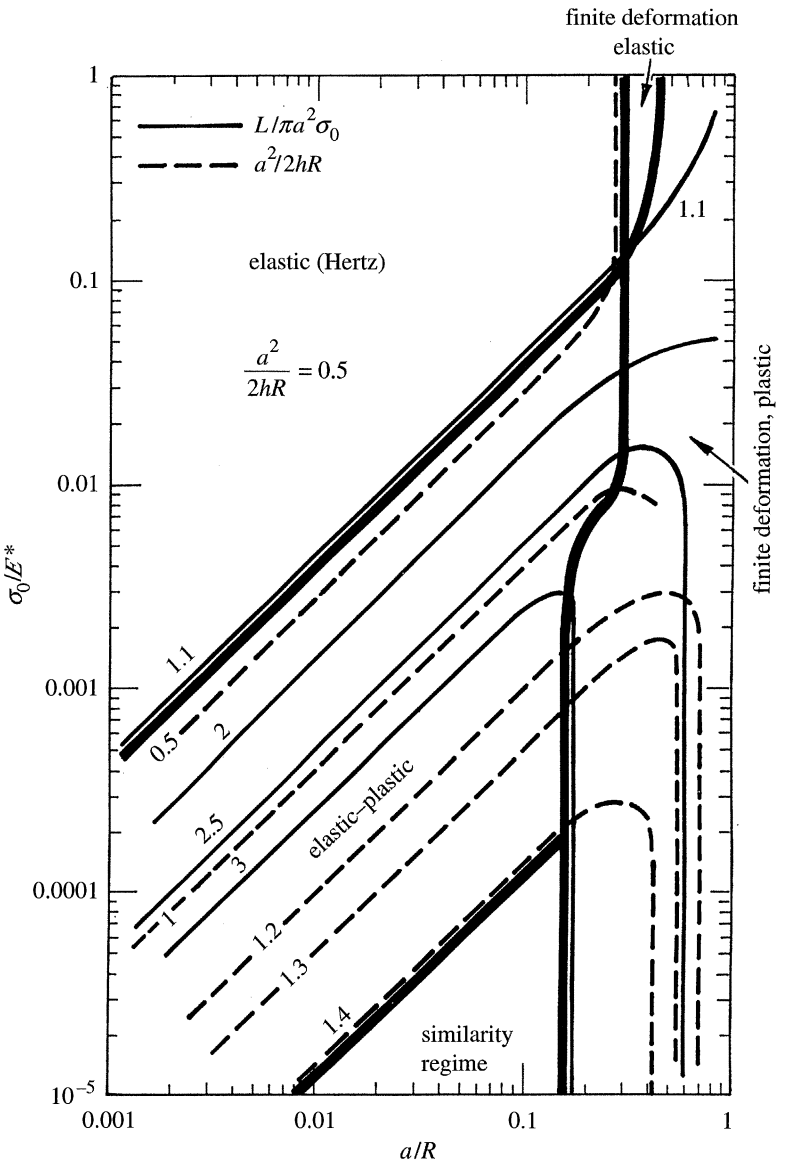

Figure 6. Map of frictionless indentation of an elastic-ideally plastic solid, showing regimes of deformation mechanism. Contours of average pressure (——) and normalized contact area $a^2/(2hR)$ (– – –) are included. The map is based on the finite-element results for $E^*/\sigma_0 = 3$, 10, 30, 100, 250, 500, 1000 and 10 000.

The map shows the evolution in indentation response with increasing contact size a/R, for any given prescribed value of yield strain σ_0/E^*. Consider, for example, indentation of a half-space of yield strain $\sigma_0/E^* = 10^{-4}$. Then, as a/R increases, the indentation response evolves from Hertz's elastic solution to the elastic-plastic solution as elucidated by Johnson (1970), to the fully plastic similarity solution, and, finally, to a state of finite-deformation plasticity.

The map comprises five distinct regimes: Hertzian elastic indentation; elastic-plastic indentation; rigid-plastic similarity regime; finite-deformation plasticity; and finite-deformation elasticity. We briefly consider each regime in turn and the factors dictating the boundaries. The Hertzian elastic regime pertains when the Mises stress within the half-space is less than the yield strength of the solid: this is satisfied for $a/R < 2.5\sigma_0/E^*$. Within the Hertzian regime, the normalized contact area is constant at $a^2/2hR = 0.5$, and the average contact pressure is given by

$$\frac{L}{\pi a^2 \sigma_0} = \frac{4}{3\pi}\frac{a}{R}\frac{E^*}{\sigma_0}.$$

Thus, along the boundary between the Hertzian regime and the elastic-plastic regime we have $L/\pi a^2\sigma_0 = 1.1$ and $a^2/2hR = 0.5$.

At very large values of yield strain, $\sigma_0/E^* > 0.1$, the Hertz solution is interrupted at large contact sizes not by the onset of yield but by finite-deformation effects; these are due to nonlinear strain–displacement kinematics and a failure of the contact assumption concerning a prescribed normal velocity. At still larger contact sizes the finite-deformation elastic regime gives way to finite-deformation plasticity.

Now consider the elastic-plastic indentation regime. Within this regime, the normalized contact pressure $L/\pi a^2\sigma_0$ and the normalized contact area $a^2/2hR$ increase with increasing combined parameter $aE^*/R\sigma_0$, as commented upon already in connection with figure 5*a*, *c*. For σ_0/E^* less than about 2×10^{-4}, the elastic-plastic regime is superseded by the similarity regime according to the criterion

$$\frac{a}{R} > 800\frac{E^*}{\sigma_0}.$$

If, on the other hand, σ_0/E^* exceeds approximately 2×10^{-4}, the elastic-plastic regime gives way to the finite-deformation plasticity regime at about $a/R = 0.16$.

Note that the similarity regime is defined as the region of the map over which the average indentation pressure *and* the normalized contact area are given by the constant values associated with the rigid-plastic similarity solution, relations (1.2 *a*), (1.2 *b*). It is bounded on the left by elasticity effects on the normalized contact area $a^2/2hR$, and on the right by finite-deformation effects on the average pressure.

4. Indentation of elastic-hardening solids by a frictionless sphere

Practical engineering alloys strain harden in the plastic range, and so it is instructive to explore the effects of strain hardening on the indentation response, for an idealized strain-hardening solid as characterized by (2.1) and (2.2). On noting that the similarity solution (1.2 *a*) states that the average indentation pressure scales with the reference stress $\sigma_r = \sigma_0[a/(\varepsilon_0 R)]^{1/m}$, we present results for the average pressure by normalizing stresses with respect to σ_r. Predictions for the *reduced average pressure* $L/\pi a^2\sigma_r$ are given in figure 7*a*, and for the normalized contact area $a^2/2hR$ in figure 7*b*, for selected values of yield strain and Poisson's ratio, and for $m = 3$.

It is clear from figure 7*a* that $L/\pi a^2\sigma_r$ increases with increasing $aE^*/R\sigma_0$ in the elastic-plastic regime and then remains constant, attaining the value predicted by the similarity solution. The differences in response for the Ramberg–Osgood and linear/power-law solids are significant only within the elastic-plastic regime. No drop in reduced average pressure is observed at large contact sizes for $m \leqslant 3$; for $m > 3$, the

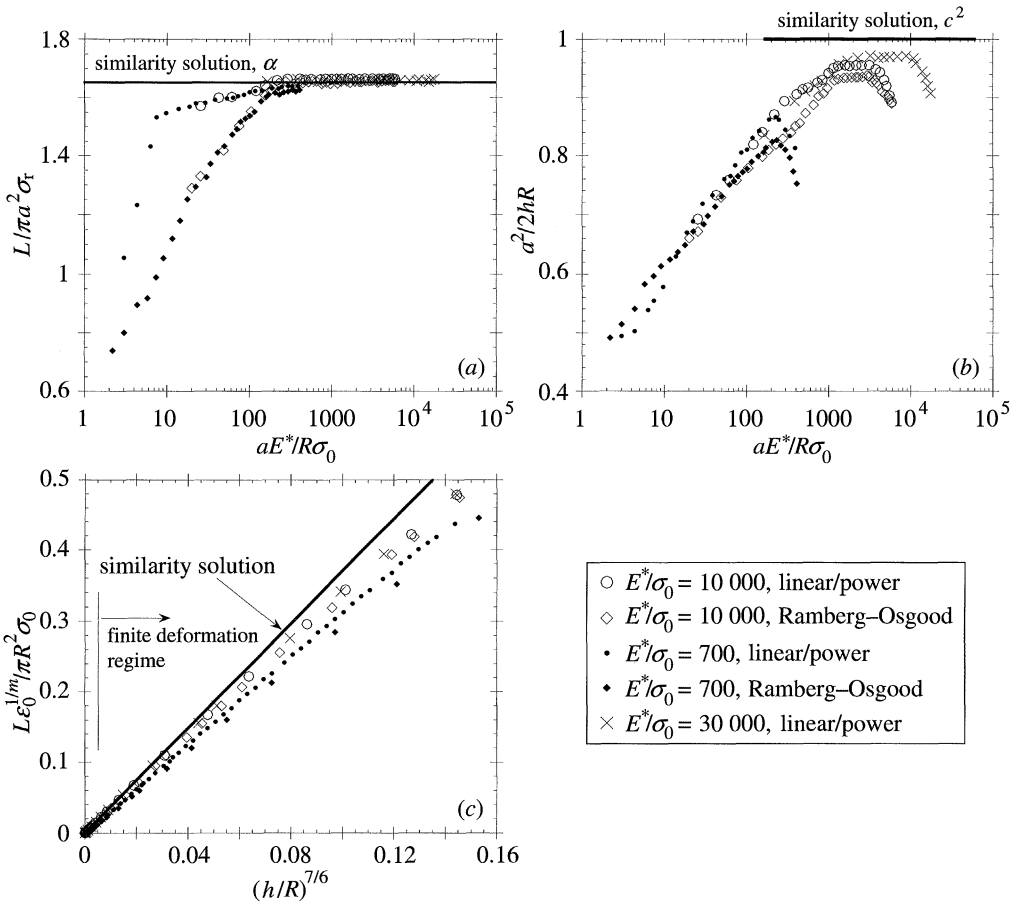

Figure 7. Indentation of elastic-plastic hardening solid, $m = 3$. (a) Reduced average pressure $L/(\pi a^2\sigma_r)$ versus $aE^*/(R\sigma_0)$; (b) normalized contact area $a^2/(2hR)$ versus $aE^*/(R\sigma_0)$; (c) load versus indent depth response.

reduced average pressure drops with increasing contact size in the finite-deformation regime. This is consistent with the feature that the similarity solution predicts a switch between sink-in and pile-up behaviour at $m = 3$; pile-up and the drop in the average reduced pressure are both associated with the plastic flow of material around the indenter.

The evolution of the normalized contact area $a^2/2hR$ with contact size (figure 7b) for the strain-hardening case ($m = 3$) is qualitatively the same as in the elastic-ideally plastic case (figure 5b, d). To within numerical error, the similarity solution is attained only for very low values of yield strain (less than 3×10^{-4}). The parameter $a^2/2hR$ increases in the elastic-plastic regime, remains constant in the fully plastic similarity regime and, then decreases again in the finite-deformation regime. The precise form of the elastic-plastic coupling in the constitutive laws (2.1) and (2.2) has a significant effect on the response within the elastic-plastic regime. Consistently, at fixed value of aE^*/σ_0, the linear/power-hardening law (2.1) gives larger values of $a^2/2hR$ and of $L/\pi a^2\sigma_r$ than the Ramberg–Osgood description (2.2). It is further noted from figure 7a, b that the combined parameter $aE^*/R\sigma_0$ adequately captures

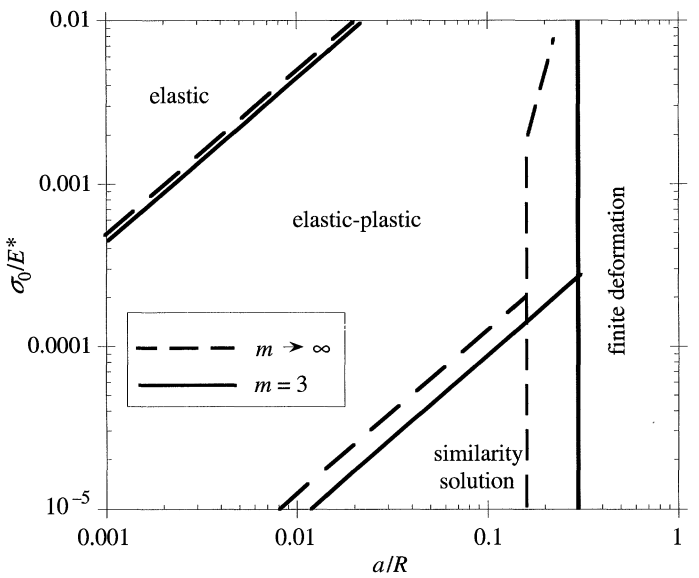

Figure 8. Comparison between the indentation maps for linear/power-law hardening solid ($m = 3$), and an elastic-ideally plastic solid.

the role of elasticity in the indentation response: curves for a range in value of yield strain and Poisson ratio coalesce within the elastic-plastic and the similarity regimes.

The similarity solution predicts that, for $m = 3$, the indentation load L is proportional to the indent depth h to the power of 7/6 (see relations (1.2*a*) and (1.2*b*)). Numerical results for L versus $h^{7/6}$ show that this contact law breaks down within the finite-deformation regime (figure 7*c*), but the deviation from the similarity solution is less pronounced then in the elastic-ideally plastic case (figure 5*e*). It is further noted from figure 7*c* that the Ramberg–Osgood constitutive law (2.2) gives a somewhat softer response than the linear/power-law version (2.1).

A comparison of the indentation map for the linear/power-law solid (2.1) with $m = 3$ and for the elastic-ideally plastic solid is given in figure 8. Overall, there is only a minor effect of strain-hardening rate on the location of the boundaries of the map. For $m = 3$, the boundaries of the similarity regime are determined solely by the behaviour of the normalized contact area $a^2/2hR$. The reduced average pressure is constant for a much wider range of contact sizes than is $a^2/2hR$ (compare figure 7*a* with figure 7*b*). In contrast, for higher values of m (such as $m = 7$ and $m \to \infty$ explored in detail), a drop in reduced average pressure occurs at a sufficiently large contact size and determines the right-hand boundary of the similarity region.

5. Effect of friction on indentation of an elastic-ideally plastic solid

In practical indentation tests it is difficult to control the degree of friction between indenter and half-space. Here, we consider the two limiting cases of frictionless indentation and sticking friction, in order to gauge the sensitivity of the indentation response to friction level. We focus our attention on indentation of an elastic-ideally plastic solid, and give some representative results in figure 9*a–c* for a solid of low yield strain ($E^*/\sigma_0 = 10\,000$, $\nu = 0.3$). Selected calculations show that the broad

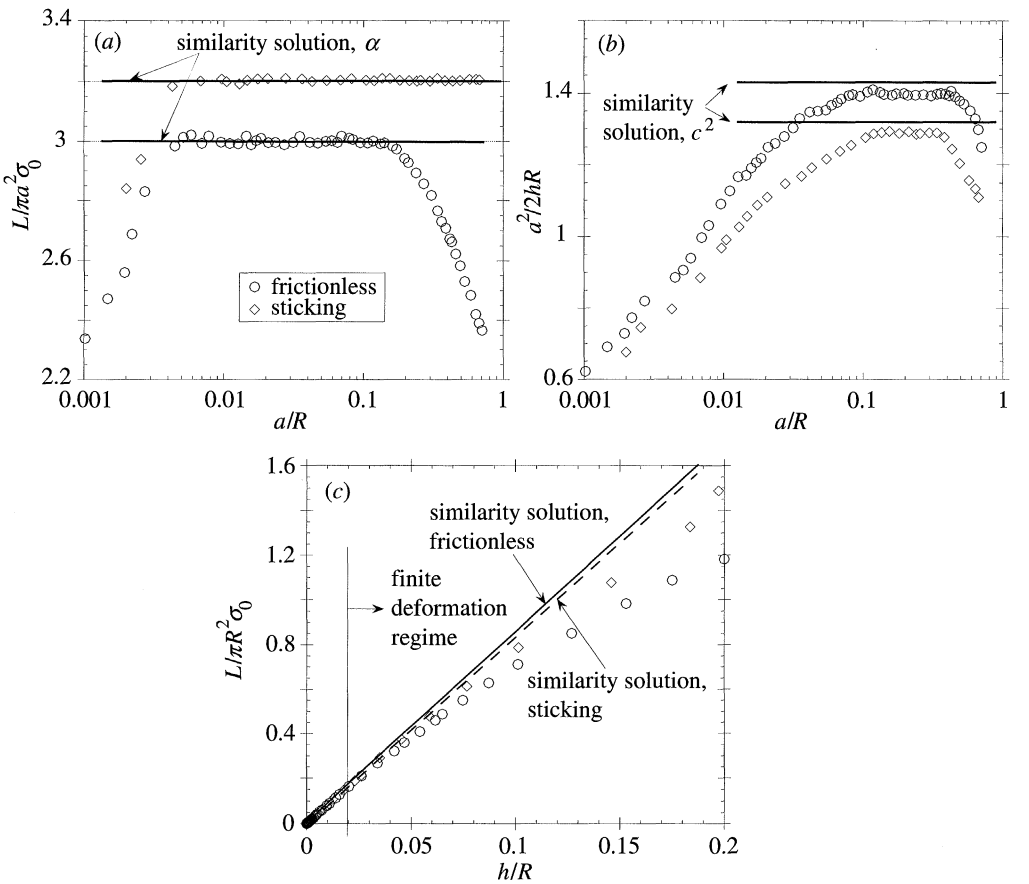

Figure 9. Comparison of frictionless and sticking indentation of an elastic-ideally plastic solid with $E^*/\sigma_0 = 10\,000$ and $\nu = 0.3$. (*a*) Average pressure versus contact size a/R; (*b*) normalized contact area $a^2/(2hR)$ versus a/R; (*c*) load versus indent depth response.

conclusions do not change for other values of yield strain and for the strain-hardening case. The similarity solutions for the frictionless and sticking indentation of the rigid-ideally plastic solid (Bower *et al.* 1993) are included in the figures.

It is clear from figure 9*a* that the average indentation pressure is consistently higher for the case of sticking friction than for the case of frictionless indentation, consistent with the notion that sticking friction induces greater plastic constraint on the deformation field. The most striking difference between the responses is the lack of a drop in the average pressure for the case of a sticking indenter in the finite-deformation regime. In the frictionless case it is the large sliding and associated material flow around the indenter that is responsible for the drop in average pressure. Now consider the normalized contact area, plotted against contact size in figure 9*b*. Compared with the frictionless case, sticking friction reduces the amount of pile-up at the edge of the indenter and leads to consistently smaller contact areas for a given indent depth. This is supported by the experimental measurements of Stute (1978), who compared the surface profiles for lubricated and dry Brinell indentation.

In contrast with the average contact pressure, the normalized contact area drops

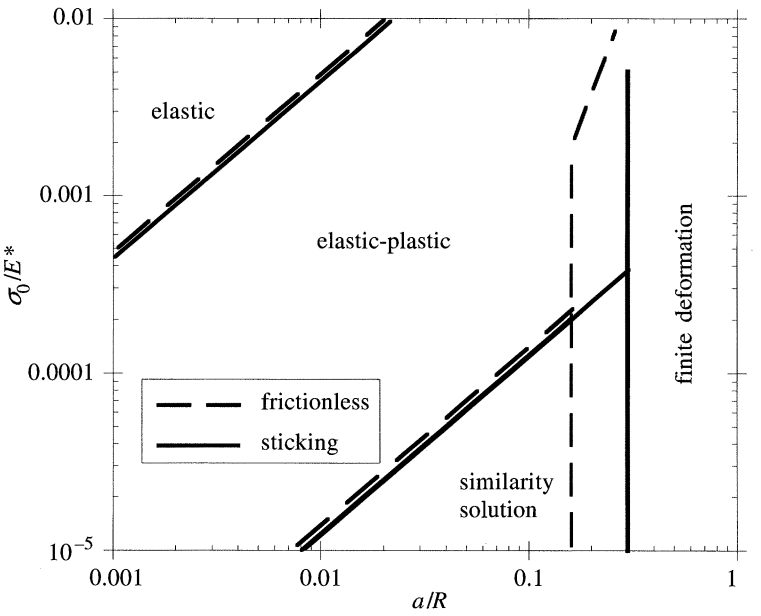

Figure 10. Comparison between the indentation maps for frictionless and sticking indentation of an elastic-ideally plastic solid.

somewhat with increasing contact size in the finite-deformation plasticity regime for the case of sticking friction. We conclude from figure 9*a*, *b* that with increasing contact size, the deformation regime evolves from elastic-plastic to the similarity regime, and, finally, to finite-deformation plasticity. Within the similarity regime, sticking friction gives 7% higher contact pressure and 8% smaller contact area than the frictionless indenter; consequently, the contact stiffness L/h by the similarity solution is about 1% greater for the frictionless case than for the sticking case. At indent depths greater than $h/R = 0.02$, the finite-deformation regime is entered and the contact stiffness decreases in a nonlinear manner with increasing indent depth (see figure 9*c*). Within this regime, the contact stiffness for the frictionless indenter is less than that for the sticking case.

An indentation map for the sticking indenter can be overlaid on that for the frictionless indenter, as shown in figure 10. The differences between the two maps are small. The finite-element predictions for the onset of first yield for the sticking indenter almost coincide with those for the frictionless indenter, in agreement with the analytical results of Hertz, Mossakovski (1963) and Spence (1968). (The detailed stress fields for the case of the sticking indenter are given by Hills & Sackfield (1987).) For both the frictionless and the sticking cases, first yield occurs at a depth of about $0.5a$. The main difference between the maps is the location of the upper boundary of the similarity regime. For the sticking case, this is determined by the breakdown of the geometric similarity condition ($a^2/2hR$ = const.), while for the frictionless case, the boundary is set by the drop in average pressure. Thus, the transition to the finite-deformation regime occurs at a higher value of a/R for the sticking indenter.

Although the friction condition has little effect on the indent force versus depth relationship, it does have a major effect on the strain distribution beneath the inden-

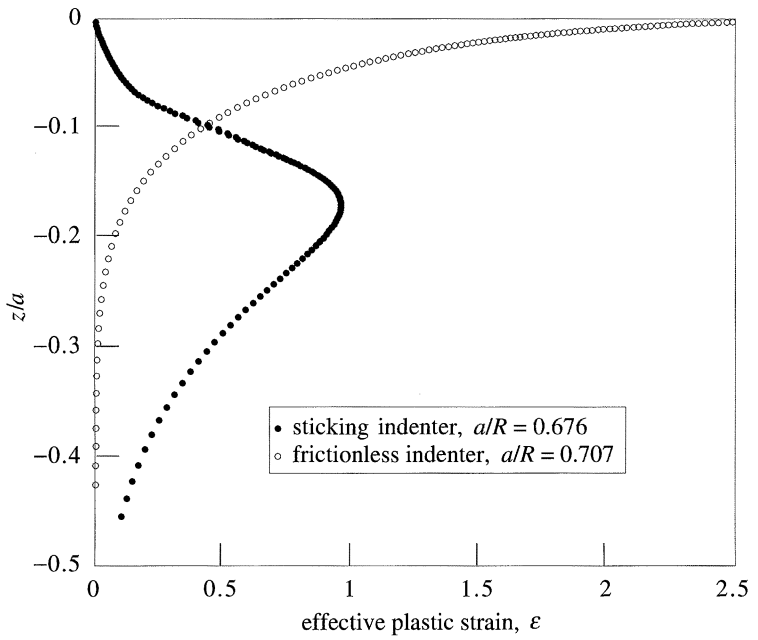

Figure 11. Distribution of effective plastic strain along the centreline and beneath the indenter, for frictionless and sticking indentation of an elastic-ideally plastic solid with $E^*/\sigma_0 = 10\,000$ and $\nu = 0.3$.

ter. For both the sticking and frictionless cases, figure 11 shows the effective plastic strain within the indented half-space, plotted as a function of depth and along the axis of symmetry. The sticking indenter imposes a radial constraint on the material in the immediate vicinity of contact; for the frictionless case, the material slides freely along the indenter and the maximum effective plastic strain occurs at the surface. Chaudhri (1996) performed a series of Vickers indentations on the cross-section of the previously spherically indented annealed copper specimen. He found that the maximum hardness (and, thus, the maximum effective strain) occurs at a depth of about $0.2a$ beneath the indenter, and not at the surface. Our results indicate that this is a friction effect.

6. The role of pre-existing stress within the half-space

Engineering surfaces often contain residual stress. For example, shot peening and ion implantation result in equibiaxial compressive stress in a surface layer, while surface thermal quenching associated with grinding and welding operations generates tensile residual stresses. Little theoretical work has been reported on the effect of these residual stresses on the indentation response. Here, we conduct a preliminary study on the effects of pre-existing stresses on frictionless indentation. For simplicity, we assume that a uniform state of equibiaxial stress exists throughout an elastic-ideally plastic half-space. Thereby, we preserve the axisymmetric nature of the problem. The assumption of uniform stress state is representative of cases where the depth of indentation is much less than the length-scale over which the residual stress field varies.

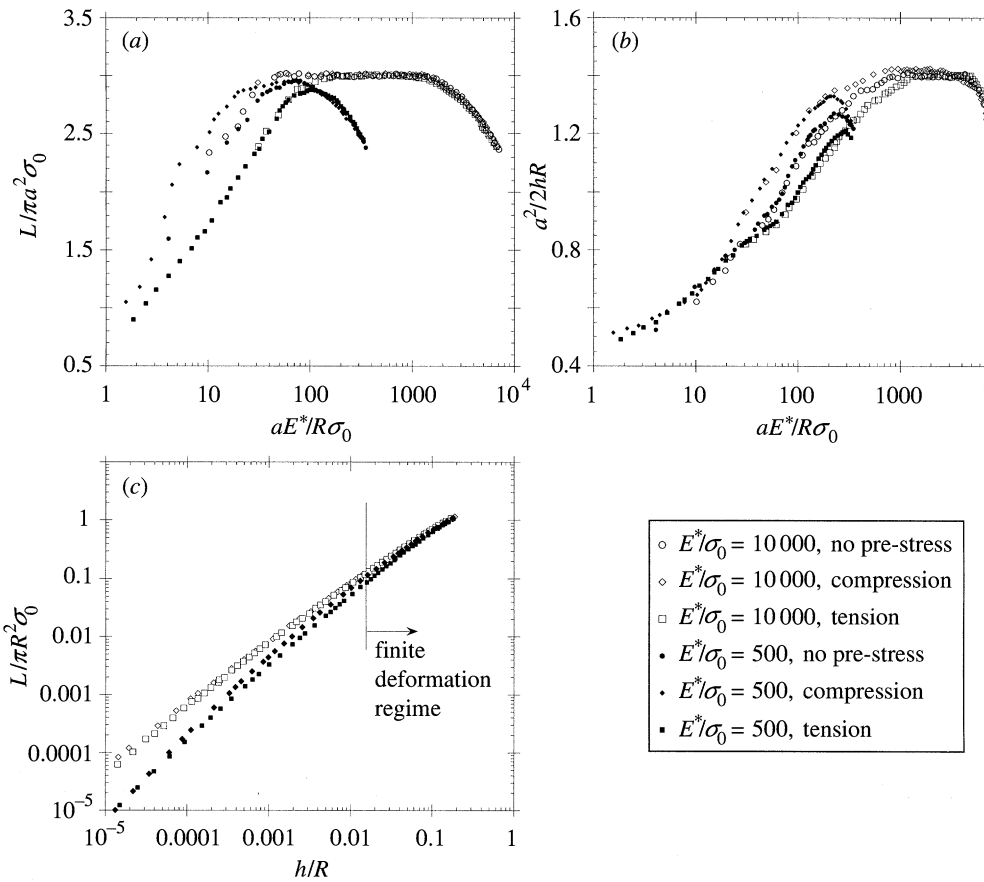

Figure 12. Effect of equibiaxial pre-stress of magnitude $\pm\frac{1}{2}\sigma_0$ in an elastic-ideally plastic half-space, with $\nu = 0.3$. (*a*) Average pressure versus $aE^*/(R\sigma_0)$; (*b*) $a^2/(2hR)$ versus $aE^*/(R\sigma_0)$; (*c*) load versus indent depth response.

Indentation predictions are given in figure 12*a–c*, for the elastic-ideally plastic solid with selected values of yield strain and $\nu = 0.3$. In each figure, predictions are shown for the cases of vanishing pre-stress, equibiaxial tension of magnitude $\frac{1}{2}\sigma_0$ and equibiaxial compression of magnitude $-\frac{1}{2}\sigma_0$. For both the similarity regime and the finite-deformation plasticity regime of indentation, pre-existing stress has a negligible effect on the average contact pressure (figure 12*a*), on the normalized contact area (figure 12*b*), and on the contact stiffness (figure 12*c*). However, within the elastic-plastic indentation regime, the average contact pressure and normalized contact area decrease with increasing residual tension, while the contact stiffness is approximately independent of the initial stress state.

The reason for the lack of an effect of pre-stress on the behaviour within the similarity regime and in the finite-deformation regime is perhaps not immediately obvious. Some insight is gained from a contour plot of effective plastic strain beneath the frictionless indenter for the three cases of equibiaxial tension, compression and vanishing initial stress (figure 13). Contours are given at an indentation state $a/R = 0.7$ within the finite-deformation regime, in a solid of low yield strain, $E^*/\sigma_0 = 10\,000$

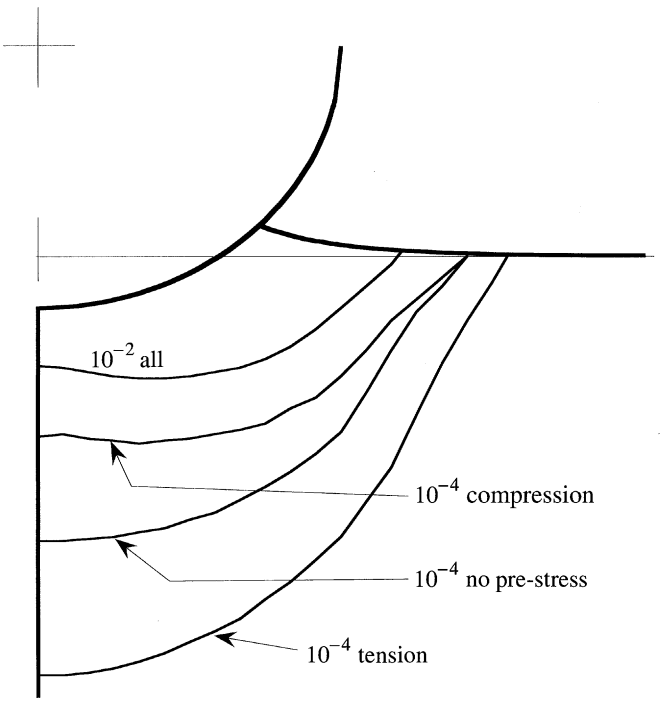

Figure 13. Contours of effective plastic strain in an elastic-ideally plastic solid of $E^*/\sigma_0 = 10\,000$ and $\nu = 0.3$, indented to a contact size of $a/R = 0.7$. Results are shown for vanishing pre-stress, and for uniform equibiaxial pre-stress of magnitude $\pm\frac{1}{2}\sigma_0$.

and $\nu = 0.3$. The contour of effective plastic strain equal to 0.0001 can be considered to be an approximate boundary of the plastic zone. While the overall plastic zone shape depends upon the level of pre-stress, the region of large strain (effective strain greater than 0.01) is practically identical in all three cases. Thus, pre-stress only has an effect in the vicinity of the elastic-plastic boundary, where elastic and plastic strains are of similar magnitude.

7. Concluding discussion

We have shown that it is the finite-deformation regime that is relevant to practical ball indentation tests and not the similarity regime. In the light of these results, it is of interest to review conventional understanding of indentation theory.

Tabor (1951) concluded that the average contact pressure is related to the contact radius by a power law with the same power as the uniaxial stress–strain law:

$$\frac{L}{\pi a^2 \sigma_0} \propto \left(\frac{a}{R}\right)^{1/m}.$$

This appears to contradict our results within the finite-deformation regime for materials with weak hardening, $m > 3$. We can explain the discrepancy as follows. First, Tabor's conclusions are based largely on O'Neill's (1944) and Meyer's (1908) load–contact size logarithmic plots, in which the slope, $k = 2 + (1/m)$, is rather insensitive to small changes in the hardening exponent. The difference between the predicted

exponents k in our work and Tabor's exponents is less than the experimental scatter in O'Neill's experiments. Second, we have shown that sticking friction can prevent the drop in average pressure within the finite-deformation regime.

The experimental data of Norbury & Samuel (1928) has been used by Tabor (1951) and by Hill *et al.* (1989) to support the idea that the similarity regime dominates the indentation response: Norbury & Samuel (1928) found that the ratio of pile-up δ to the indent depth h is constant. Their experimental data are for $a/R > 0.4$, and relate to the finite-deformation regime. Our numerical results (not shown) also indicate that δ/h is constant within the finite-deformation regime.

We conclude by listing the main findings and implications of the current study as follows.

(i) The region of validity of the plastic similarity solution is severely limited by elastic effects for small contacts, and by finite-deformation effects for large contacts. Maps of indentation regimes can be generated in a straightforward manner to provide guidance for future testing and interpretation. The boundaries of the indentation regimes are relatively insensitive to the degree of strain hardening and to the level of interfacial friction.

(ii) The level of friction strongly affects the strain field beneath the indenter, and has a quantitative effect on the contact size as a function of indent depth. Within the similarity regime, the contact stiffness is almost the same for sticking and for frictionless indentation.

(iii) Pre-existing stress within the half-space has a minor effect on the indentation response, except for the elastic-plastic indentation regime.

(iv) Extraction of material parameters, such as the hardening exponent m and the characteristic strength σ_0, is feasible from load versus indent depth measurements, but may require more sophisticated indentation measurements than those currently practised.

The authors are grateful for financial support from the NIST, contract number 70-NAN-B5H-0042, and for helpful technical discussions with Dr R. J. Fields of the NIST. The authors also acknowledge helpful comments by Professor K. L. Johnson and Dr M. M. Chaudhri.

References

ABAQUS 1995 *V5.5 user's manual.* Pawtucket, RI: Hibbitt, Karlsson & Sorensen Inc.

ASTM 1993 ASTM Standards E10-84 and E18-89a. *Annual book of ASTM standards.* Philadelphia, PA: ASTM.

Biwa, S. & Storåkers, B. 1995 An analysis of fully plastic Brinell indentation. *J. Mech. Phys. Solids* **43**, 1303–1334.

Bower, A. F., Fleck, N. A., Needleman, A. & Ogbonna, N. 1993 Indentation of power law creeping solids. *Proc. R. Soc. Lond.* A **441**, 97–124.

Chaudhri, M. M. 1987 The plastic deformation of single asperities by hard flats. *Inst. Mech. Engng Conf. Publ.* C **158**, 1003–1012.

Chaudhri, M. M. 1996 Subsurface plastic strain distribution around spherical indentation in metals. *Phil. Mag.* A **74**, 1213–1224.

Chaudhri, M. M., Hutchings, I. M. & Makin, P. L. 1984 Plastic compression of spheres. *Phil. Mag.* A **49**, 493–503.

Fleck, N. A., Otoyo, H. & Needleman, A. 1992 Indentation of porous solids. *Int. J. Solids Struct.* **29**, 1613–1636.

Follansbee, P. S. & Sinclair, G. B. 1984 Quasi-static normal indentation of an elasto-plastic half-space by a rigid sphere. I. *Int. J. Solids Struct.* **20**, 81–91.

Hardy, C., Baronett, C. N. & Tordion, G. V. 1971 The elasto-plastic indentation of a half-space by a rigid sphere. *Int. J. Num. Methods* **3**, 451–462.

Hill, R. 1992 Similarity analysis of creep indentation tests. *Proc. R. Soc. Lond.* A **436**, 617–630.

Hill, R., Storåkers, B. & Zdunek, A. B. 1989 A theoretical study of the Brinell hardness test. *Proc. R. Soc. Lond.* A **436**, 301–330.

Hills, D. A. & Sackfield, A. 1987 The stress field induced by normal contact between dissimilar spheres. *J. Appl. Mech.* **54**, 8–14.

Hills, D. A., Nowell, D. & Sackfield, A. 1993 *Mechanics of elastic contact.* Oxford: Butterworth-Heinemann.

Johnson, K. L. 1970 The correlation of indentation experiments. *J. Mech. Phys. Solids* **18**, 115–126.

Johnson, K. L. 1985 *Contact mechanics.* Cambridge University Press.

Kral, E. R., Komvopuolos, K. & Bogy, D. B. 1993 Elastic-plastic finite element analysis of repeated indentation of half-space by a rigid sphere. *J. Appl. Mech.* **60**, 829–841.

Kral, E. R., Komvopuolos, K. & Bogy, D. B. 1995*a* Finite element analysis of repeated indentation of an elastic-plastic layered medium by a rigid sphere. Part I. Surface results. *J. Appl. Mech.* **62**, 20–28.

Kral, E. R., Komvopuolos, K. & Bogy, D. B. 1995*b* Finite element analysis of repeated indentation of an elastic-plastic layered medium by a rigid sphere. Part II. Subsurface results. *J. Appl. Mech.* **62**, 29–42.

Laursen, T. A. & Simo, J. C. 1992 A study of the mechanics of microindentation using finite elements. *J. Mater. Res.* **7**, 618–626.

Mesarovic, S. Dj. & Fleck, N. A. 1999 The contact between viscoplastic and rigid spheres. *Int. J. Solids Struct.* (In the press.)

Meyer, E. 1908 Untersuchungen über Harteprufung und Harte. *Z. Ver. Deutche Ing.* **52**, 645–654.

Mossakovski, V. I. 1963 Compression of elastic bodies under conditions of adhesion (axisymmetric case). *PMM* **27**, 418–427.

Norbury, A. L. & Samuel, T. 1928 The recovery and sinking-in or piling-up of material in the Brinell test, and the effects of these factors on the correlation of the Brinell with certain other hardness tests. *J. Iron Steel Institute* **117**, 673–687.

Ogbonna, N., Fleck, N. A. & Cocks, A. C. F. 1995 Transient creep analysis of ball indentation. *Int. J. Mech. Sci.* **37**, 1179–1202.

O'Neill, H. 1944 The significance of tensile and other mechanical test properties of metals. *Proc. Inst. Mech. Engineers* **151**, 116–130.

Sharp, S. J., Ashby, M. F. & Fleck, N. A. 1993 Material response under static and sliding indentation loads. *Acta Metall. Mater.* **41**, 685–692.

Spence, D. A. 1968 Self similar solutions to adhesive contact problems with incremental loading. *Proc. R. Soc. Lond.* A **305**, 55–80.

Stute, H. 1978 Investigations about the influence of grease on the Brinell hardness of steel. *VDI-Berichte* **308**, 185–190.

Tabor, D. 1951 *The hardness of metals.* Oxford University Press.

Timothy, S. P., Pearson, J. M. & Hutchings, I. M. 1987 The contact pressure distribution during plastic compression of lead spheres. *Int. J. Mech. Sci.* **29**, 713–719.